



HAL
open science

Electronic Structures of the MoS₂/TiO₂ (anatase) Heterojunction: Influence of Physical and Chemical Modifications at the 2D-or 1D Interfaces

Rémi Favre, Pascal Raybaud, Tangui Le Bahers

► **To cite this version:**

Rémi Favre, Pascal Raybaud, Tangui Le Bahers. Electronic Structures of the MoS₂/TiO₂ (anatase) Heterojunction: Influence of Physical and Chemical Modifications at the 2D-or 1D Interfaces. *Physical Chemistry Chemical Physics*, 2022, 24 (4), pp.2646-2655. 10.1039/D1CP05151B . hal-03586087

HAL Id: hal-03586087

<https://ifp.hal.science/hal-03586087>

Submitted on 23 Feb 2022

HAL is a multi-disciplinary open access archive for the deposit and dissemination of scientific research documents, whether they are published or not. The documents may come from teaching and research institutions in France or abroad, or from public or private research centers.

L'archive ouverte pluridisciplinaire **HAL**, est destinée au dépôt et à la diffusion de documents scientifiques de niveau recherche, publiés ou non, émanant des établissements d'enseignement et de recherche français ou étrangers, des laboratoires publics ou privés.



Distributed under a Creative Commons Attribution - NonCommercial 4.0 International License

Electronic structures of the MoS₂/TiO₂ (anatase) heterojunction: influence of physical and chemical modifications at the 2D- or 1D-interfaces.

Rémi Favre,^a Pascal Raybaud,^{a,b,*} and Tangui Le Bahers^{a,*}

To tackle the challenge of the CO₂ photoreduction, semiconducting layered transition metal dichalcogenides like MoS₂ have attracted much attention due to their tunable 2D nano-structures. By using advanced periodic density functional theory calculations (HSE06 functional), we provide a systematic quantification of the optoelectronic properties of various interfacial heterostructures between MoS₂ and anatase TiO₂. We systematically determine the band gaps, conduction bands (CB) and valence bands (VB) positions to figure out the nature of the heterojunction. Two main surface orientations of anatase TiO₂ particles, (101) and (001), are considered with 2D-MoS₂ nanosheet or nanoribbon either through a 2D physical (van der Waals) or through a 1D chemical interface. The possibility to chemically modify the MoS₂/TiO₂ interface, either by sulfidation or hydration, and its effect on the electronic structure are deeply investigated. These modifications in the heterostructure lead to important changes in the electronic properties and charge transfer between the two materials which impact both photon absorption properties and charge carriers dynamics suspected to influence in turn the photocatalytic activity. While a type I heterojunction is found for the 1D chemical interface, a type II heterojunction with appropriate CB/VB positions for CO₂ reduction and H₂O oxidation is identified for the 2D physical interface which could lead to the targeted Z-scheme mechanism with strong potential interest in photocatalysis applications.

Introduction

Motivated by the fruitful progress of the research on the photocatalytic water splitting to produce H₂¹⁻³, the strong interest for CO₂ photoreduction into solar fuels is growing within the community of heterogeneous photocatalysis^{4,5} for economic and ecological interests. Unfortunately, this topic appears to be much more challenging for several reasons. Carbon dioxide is involved in many oxidation-reduction couples and could be reduced in different valuable products (CH₄, CH₃OH, HCOOH, CO...) prompting the control of the selectivity depending on the targeted process. Moreover, these reactions are involving a high number of electrons (up to 8). Last but not least, the CO₂ reduction mechanism is still unclear and could require a large electrochemical potential to perform the first electron transfer. All of this leads to the actual systems with an energy conversion efficiency around 1%⁶, far from the targeted value of 10%⁷.

In order to tackle the challenging development of photocatalytic CO₂ reduction, numerous studies are exploring

various classes of promising semiconducting materials that could offer new perspectives in the photocatalysis research. Among these materials, transition metal dichalcogenides, such as MoS₂ is attracting attention for its strong stability (against air, oxygen and sulfur) and its optoelectronic properties adapted for photocatalysis, as highlighted by several experimental works^{8,9}. Moreover, this 2D material presents a nano-structures that could be easily tuned (doping elements, number of layers, size of the nanosheet...) in order to adapt its optoelectronic properties as a function of the requirements¹⁰. However, the limitation of the use of MoS₂ in photocatalysis may raise from its slightly too small bandgap (between 1.3¹¹ and 1.9¹² eV as a function of the number of layers). As an example, to realize efficiently the photoreduction of CO₂ in HCOOH at pH=0 with H₂O as the reducer, a bandgap higher than 2.1 eV would be necessary with properly tuned positions of the conduction and valence bands (CB/VB)⁵.

To overcome this challenge, the possibility of a Z-scheme mechanism¹³⁻¹⁴ based on the interaction of MoS₂ with another well-chosen semiconductor is often explored. This specific mechanism could be made possible by the use of type II heterojunction (**Fig.1**), where the absorption of two photons is followed by an electron-hole recombination at the interface between the two semiconductors. In a Z-scheme working principle, the interface built between two small bandgap materials, allows to reach highly reactive and spatially

^a Univ Lyon, ENS de Lyon, CNRS, Université Claude Bernard Lyon 1, Laboratoire de Chimie UMR 5182, F-69342, France

^b IFP Energies Nouvelles, Rond-point de l'échangeur de Solaize, BP 3, 69360 Solaize, France

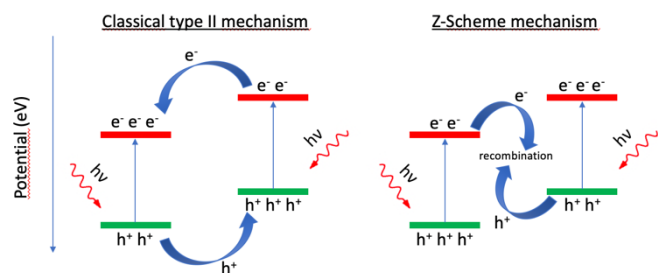


Fig. 1 Comparison of the classical type II mechanism and the Z-scheme mechanism

separated charge carriers. The choice of the second semiconductor is thus driving not only the band gap itself but also by the relative positions of the conduction and valence bands (CB/VB). The orientation towards a classical type II mechanism or a Z-scheme depends on various factors such as band bending, interfacial electric field or the dynamics of charge transfer which are challenging parameters to control.¹³⁻¹⁴

Due to the low-cost, high stability and abundance of the 2H-MoS₂ and anatase-TiO₂ materials, MoS₂/TiO₂ heterostructure has been the subject of numerous studies¹⁵⁻¹⁶ combining the efficient photocatalytic properties of TiO₂¹⁷⁻¹⁸ with the well-known catalytic activity of MoS₂ for the activation, conversion and production of various molecules¹⁹⁻²⁰. The loaded MoS₂ may act as a cocatalyst with the aim to harvest the photogenerated charges in order to avoid the recombination of the electrons and holes photogenerated in TiO₂. The charge carriers collected and the active sites of MoS₂ offers a large range of applications (degradation of organic pollutants²¹⁻²², CO₂ reduction²³, Hydrogen Evolution Reaction²⁴...). In general, investigations on MoS₂/TiO₂ nano composites are focusing on the Hydrogen Evolution Reaction. Efficient nano composites are composed of MoS₂ nanosheets coated on TiO₂ in a core-shell structure. The TiO₂ core could have different shapes (nanowire²⁵, nanobelt²⁶ or nanotubes²⁷). Since the (101) surface is known to be the most stable and the predominant surface²⁸⁻²⁹, it is generally proposed that the MoS₂ layers are mainly located on this surface. However, a recent study focusing on a 2D MoS₂ monolayer deposited on the (001) surface of anatase TiO₂ nanosheet³⁰, revealed that photocatalytic activity in H₂ evolution from water is 36.4 times higher than on pure TiO₂ nanosheet and even 2 times higher than Pt/TiO₂, showing the high potential interest of MoS₂/TiO₂ as photocatalytic system. However, despite the strategies considered to increase the HER performance (MoS₂ engineering, interface engineering, use of photosensitizer or sacrificial agent), the best photoactivities obtained (16.7 mmol.g⁻¹.h⁻¹²⁵ and 2.2 mmol.g⁻¹.h⁻¹²²) are still not satisfying. From the CO₂ photoreduction point of view, the few results obtained with MoS₂/TiO₂ nanosheets are promising with an activity of 10.6 μmol.g⁻¹.h⁻¹, 3 times higher than pure TiO₂ nanosheets and 2 times higher than Pt/TiO₂ 0.5 wt% Pt²³.

As presented above, the photoactivity obtained with the MoS₂/TiO₂ heterostructure is particularly appealing but remains to be improved for several reasons. First, the mismatch between MoS₂ and TiO₂ lattice leads to a highly defective interface with only a small amount of MoS₂ in direct contact with TiO₂. Second, MoS₂/TiO₂ architectures are facing the

limitations of poor visible-light harvesting, low electrical conductivity and deficient catalytic active sites prompting the deeper optimization of the nano-structuration to overcome these drawbacks. In particular, the impact of the structure of the MoS₂/TiO₂ heterojunction (nature of the TiO₂ crystallographic facets, chemical or physical interaction between MoS₂ and TiO₂, chemical composition of the interface) on the optoelectronic properties is not known. Hence, providing a detailed atomistic description of the MoS₂/TiO₂ interface will undoubtedly open perspectives on this interface design for photocatalytic applications.

With the aim at providing rational guides for the materials' nanostructuration of the TiO₂/MoS₂ interface, we propose in the present work to explore the evolution of the band gap and conduction band (CB)/valence band (VB) positions of various 1D- or 2D-MoS₂/TiO₂-anatase heterojunctions by using state of the art periodic density functional theory (DFT) calculations. We will focus on the two main surface orientations of anatase particles ((101) and (001)). The contribution of the (001) surface orientation, neglected for its minor presence on anatase particles in vacuum conditions²⁸, could become more predominant under aqueous environment²⁹ encountered in reactions involving water as a reactant (such as water splitting). Hence, it will be also considered carefully in this work. In addition, beyond the physical van der Waals interaction, the chemical epitaxy-like interaction which has been reported in the literature³¹⁻³³ will be also investigated. Moreover, the influence of key physico-chemical parameters of the interface on the CB/VB positions will be studied: sulfidation and hydration states, orientation of the MoS₂ monolayer, size of MoS₂ monolayers.

The objective of this study is thus to provide a general view on the evolution of the band positions and the possible charge carrier pathway after the heterojunction as a function of physico-chemical parameters accessible experimentally. The feasibility of a Z-scheme mechanism, different from the classical type II mechanism presented in the actual work on MoS₂/TiO₂, will also be discussed.

Methods

DFT calculations were all performed using Vienna Ab Initio Simulation Package (VASP) code^{34,35}. Geometry optimizations were performed using the PBE functional³⁶, followed by a single point calculation using the range separated hybrid HSE06 functional³⁷ along with a cut off-energy of 500 eV. In both cases, the Van der Waals contributions were described using the Grimme D3 approach with Becke-Johnson damping (D3-BJ)³⁸. The precision setting of VASP was set to "Normal" and a Gaussian smearing 0.05 eV was used. The convergence criterion for the SCF cycle was fixed at 10⁻⁷ eV per unit cell and the maximum forces were converged to below 0.02 eV/Å during the geometry optimization. Complementary spin polarized calculations were performed when necessary (**Supporting Information 5**).

To mimic aqueous conditions, in which water could be used either as a reactant or could be produced by the redox

reactions, implicit water solvent was added in interfacial systems and independent ones using the VASPsol code³⁹.

The TiO₂ anatase (101) and the (001) surfaces were considered (**Fig. S1**). For the (001) surface, in addition to implicit water solvation (as described before), explicit hydration of the surface was used with a water coverage of 3.5 H₂O/nm² was considered because it was shown that in ambient conditions hydroxyl groups stabilize the Ti sites present on the bare surface²⁹. This effect on electronic properties has been tested as reported in the result section. A 12x12x1 k-point mesh was used for the calculations on the separated materials (TiO₂ surfaces and MoS₂ monolayer). A vacuum thickness of 20 Å was used based on convergence calculations (**Supporting Information 8**).

For the physical interaction, one infinite 2D-MoS₂ nanosheet has been chosen which is known to exhibit larger bandgap than multilayers¹⁰. For the heterojunction, the MoS₂ nanosheet was optimized in parallel orientation with respect to the TiO₂ surfaces leading to a 2D-interface. For that, the unit cell of the two materials was multiplied in order to respect the commensurability of the respective lattice parameters (**Fig. S2**). In the case of MoS₂ on TiO₂ anatase (101), we used a 5x2x1 supercell for MoS₂ on a 4x1x1 supercell for TiO₂ with a MoS₂ dilatation of 2.12% on the x axis and 4.26% on the y axis. On the (001) surface, we used a 5x3x1 supercell for MoS₂ on a 4x4x1 supercell for TiO₂ with a MoS₂ dilatation of 2.57% on the x axis and 6.60% on the y axis. Based on convergence calculations presented in **Supporting Information 8**, a reduced k-point mesh was used: 4x4x1 for the geometry optimizations at PBE-D3 level and 1x1x1 for the single point HSE06 calculations. Valence band and conduction band are determined from the last occupied state and the first unoccupied one. The Fermi level corresponds to the top of the valence band. These values are then adjusted with respect to the vacuum potential, different for each calculation, and determined by plotting the local electrostatic potential (**Fig. S3**).

For the chemical interaction, we chose one finite size MoS₂ nanoribbon exposing edges forming Mo-O-Ti or Mo-S-Ti chemical bonding along a 1D-interface with TiO₂. A tilting angle of the nanoribbon with respect to the TiO₂ surface is observed after geometry optimization. Various sizes of the nano-ribbon have been simulated. More details will be given in the results section.

In order to avoid artificial dipole moment in slab structures, symmetric slabs were modelled with one MoS₂ nanosheet added on each side of the TiO₂ slab leading to systems containing between ~300 and ~500 atoms.

We determined the electronic adhesion energies of each system. This energy descriptor aims at apprehending the relevancy and realism of the proposed systems at first order.

Due to the size of systems, an exhaustive study of absolute thermodynamic stability as a function of conditions which would include vibrational analysis is beyond the scope of this study.

Result

MoS₂ 2D-monolayer in physical interaction with TiO₂ anatase surfaces

a) Bare and hydrated TiO₂ surfaces

Before investigating the heterostructures, the influence of explicit hydration of TiO₂ surfaces on their electronic structure has been investigated proving that while the electronic structure of the (101) surface is weakly affected by water molecules, the presence of an explicit solvation by adding dissociated water on the Ti and O sites of the (001) surface has a large impact on the bandgap and VB/CB positions, which is mandatory to recover the experimental values (**Fig. S8**). A similar impact of dissociated water on rutile and anatase surfaces was reported by a previous theoretical study⁴⁰. As a matter of fact, a 3.5 H₂O/nm² coverage (i.e. 8 water molecules by unit cell adsorbed in a dissociative way) is required to reach the 3.3 eV bandgap expected for TiO₂ anatase surfaces. The (001) surface with hydration of 3.5 H₂O/nm² corresponds to the presence of one hydroxyl (OH) group per surface Ti atom, without residual molecular water²⁹. By contrast, the (101) surface was shown to stabilize non-dissociated water, with almost no influence on the bandgap. As a consequence, in what follows the bare (101) surface was modeled only while the (001) one was explicitly solvated.

As a starting point for the investigation of the TiO₂/MoS₂ heterostructures, we focused on structures with MoS₂ physically adsorbed on TiO₂, i.e. interacting by van der Waals forces and eventually also by hydrogen bonding with TiO₂ (**Fig. 2**). For these architectures, the weak interaction energies (-0.21 eV/MoS₂ for (101) and -0.10 eV/MoS₂ for (001)) and the average distance between the O plane (on the surface for (101) and on the hydroxyls for (001)) and the S plane (2.87 Å for (101) and 3.02 Å for (001)) supports the idea of a van der Waals type of interaction as reported in the literature for similar systems^{25,26,41}.

As a consequence of this weak interaction between TiO₂ and MoS₂ in a van der Waals heterostructure, the electronic structures of the interface can be seen as the sum of the electronic structures of the two individual materials (**Fig. 2**). The interface is a Type-II heterostructure (**Fig. 1**) characterized by the existence of a bandgap (1.26 eV for (101) and 1.45 eV for (001)), with a valence band located on MoS₂ and a conduction band located on TiO₂.

The density of states (DOS) with the projected states on each element (**Fig. S9**), show that the valence band is mainly localized on the Mo atoms of MoS₂ while the conduction band is localized on the Ti atoms of TiO₂. Such type of heterostructure might eventually lead to a type II or a Z-type working principle (**Fig. 1**) To complete the electronic structure characterization of these interfaces, the charge transfer will be discussed later.

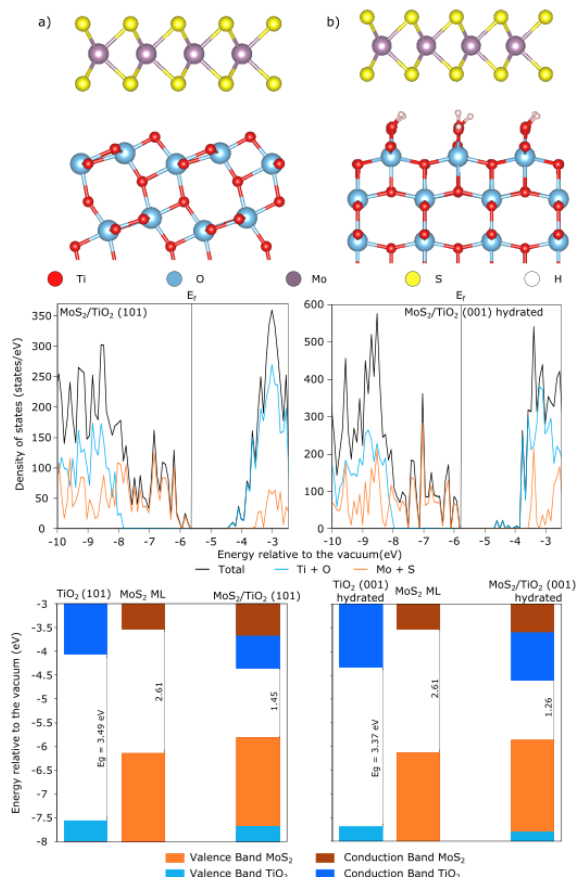


Fig. 2 Molecular structure of MoS₂ monolayer physically adsorbed, DOS of these interfaces and evolution of the band position before and after junction for a) MoS₂/TiO₂ (101) and b) MoS₂/TiO₂ (001) hydrated

b) Sulfided and hydrated-sulfided TiO₂ surfaces

Previous DFT⁴² and experimental XPS⁴³ studies showed that the TiO₂ surface may be sulfided under sulfiding conditions (using H₂S as sulfiding agent for instance). Hence, the substitution of surface oxygen atoms by sulfur atoms on TiO₂ is thermodynamically stabilized under such conditions. Being inspired by these former studies, we considered two sulfided TiO₂ surfaces (one for each orientation), as represented in **Fig. 3** with the MoS₂ monolayer physically adsorbed on. The first one (**Fig. 3a**) corresponds to a substitution of two oxygen atoms by unit cell on the (101) bare surface leading to a 1.7 S/nm² coverage on the surface. After optimizing the physical MoS₂/TiO₂-S heterostructure, the average distance between the two S planes (on the TiO₂ surface and on the MoS₂ nanosheet) is 2.73 Å and the average distance between the S plane of MoS₂ and the O plane of TiO₂ is 3.19 Å, thus larger than without sulfidation (2.87 Å), which explains the weaker adhesion energy of -0.06 eV/MoS₂.

The second one (**Fig. 3b**) considers the same hydration state as for the non-sulfided (001) surface and the substitution of the four oxygen atoms by sulfur atoms per unit cell, resulting in a coverage of 3.5 H₂O/nm² and 1.7 S/nm². After the junction with a MoS₂ the average distance between the two S planes (on the surface and on the nanosheet) is 3.42 Å (~0.7 Å greater than in the previous case) while the average distance between the S plane and the O plane is now 2.86 Å smaller than before

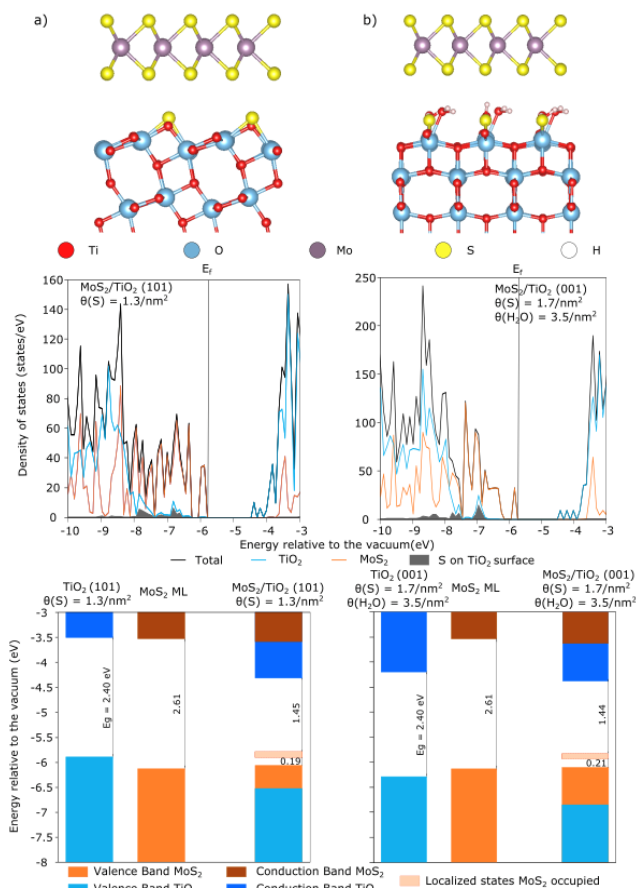


Fig. 3 Molecular structure of MoS₂ monolayer physically adsorbed, DOS of the interfaces and evolution of the band position before and after junction for a) TiO₂ (101) with $\theta(S) = 1.7$ S/nm² b) TiO₂ (001) with $\theta(S) = 1.7$ S/nm² and $\theta(H_2O) = 3.5$ H₂O/nm²

sulfidation (3.02 Å). It is explained by the fact that after optimization, 8 OH groups remain while 8 OH groups are retransformed into 4 water molecules and 4 surface oxygen, closer to the nanosheet. So, the final hydroxylation state of surface is different from the non sulfided one. The average distance between the oxygen plane of the hydroxyls and the S plane of the nanosheet is 3.12 Å (3.02 Å before sulfidation). The adhesion energy remains small (-0.10 eV/MoS₂) as in the non sulfided case, due to various compensation effects induced by van der Waals interactions and H-bonding.

The DOS with material decomposition associated to these structures (**Fig. 3**) shows that the 3p states of the sulfur atoms located on both sulfided TiO₂ surfaces are mainly contributing to the top of valence band of TiO₂, whereas the 2p states of oxygen were contributing on the non-sulfided surfaces. Moreover, the 3p S states are higher in energy (~1 to 1.5 eV) with respect to the former 2p O states.

The change of the band positions after the junction, is more pronounced than for the previous non sulfided surfaces. On the sulfided (101) surface (**Fig. 3 a**), we observe a fall of the conduction band of TiO₂ that could be driven by the sulfur-sulfur interaction across the interface. On the (001) sulfided and hydrated (**Fig. 3 b**), this interaction is diminished due to the surface hydration. In both cases, we observe after interaction a fall of the valence band of TiO₂ (localized on the surface sulfur)

and a climb of the valence band of MoS₂. The apparition of localized 4d Mo states at the top of the valence band could be induced by the shift of 3p S states of the TiO₂ surface at higher energy levels becoming closer to the top of the valence band of the MoS₂ nanosheet (than the 2p O states in the non-sulfided case).

MoS₂ nanoribbon in chemical interaction with TiO₂ anatase surfaces

a) Bare and hydrated TiO₂ surfaces

As discussed in Introduction, the literature reports the possibility to grow MoS₂ nanosheet on top of anatase particles by epitaxy³¹⁻³³. In that case, we consider a nanoribbon with infinite dimension only in the direction parallel to the TiO₂ surface forming a 1D chemical interface. On the other direction, the nanoribbon implies the creation of two different edges on MoS₂ usually called “Mo-edge” and “S-edge”⁴⁴ (Fig. 4 a). The more favorable restructuring (Fig. 4 b) corresponding to 50% sulfur atoms (with respect to bulk reference) on each edge has been chosen for building the epitaxial structure.

The creation of these edges has a strong impact on the electronic structure associated (Fig. 5) with a strong decrease (~2 eV) of the bandgap with respect to the infinite nanosheet due to new electronic states localized on the edges. As already reported by previous DFT studies⁴⁵, these electronic states filled the top of the valence bands and the bottom of the conduction bands.

Depending on the way the interfacial structure is prepared, its chemical composition or the size of the MoS₂ nanoribbon may change. Particularly, if the genesis of the MoS₂ nanoribbon is obtained through a sulfidation process of Mo-oxide precursor, some oxygen atoms may not be fully replaced by sulfur atoms at the interface and some Mo-O-Ti bridges may remain^{31,46}. Also, the size of the MoS₂ nanoribbon can be tuned by the experimental conditions such as sulfidation temperature. Changing such features have been invoked in the case of MoS₂ based catalysts⁴⁷. These chemical modifications have been tested on the finite nanoribbon (Fig. 5) but they have only a slight impact on the band positions, apart from oxygen doping which induces the apparition of a localized state and a down shift of the valence band induced by the 2p O state.

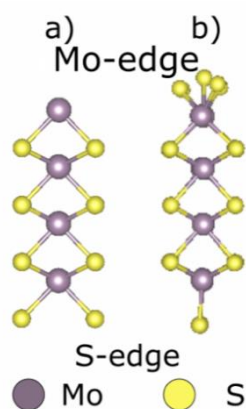


Fig. 4 Evolution of the MoS₂ finite nanoribbon before (a) and after restructuring induced by the transfer of half of S-atoms from the S-edge to M-edge (b))

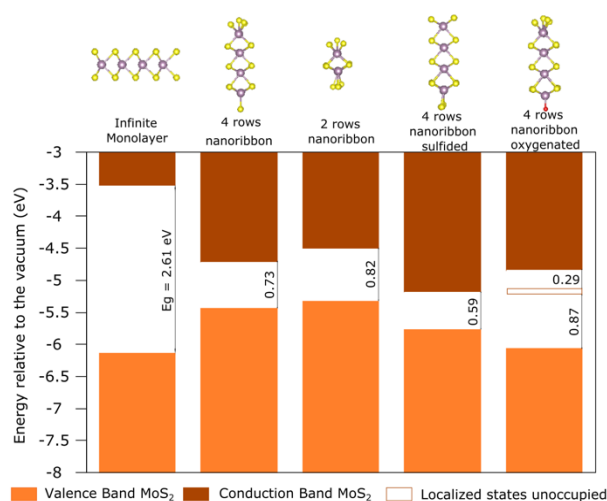


Fig. 5 Evolution of the band positions of MoS₂ when going from the monolayer to the nanoribbons and chemically modified nanoribbons

First, we focus on the ribbon without chemical modification and we explore to which extent a chemical interaction between MoS₂ and TiO₂ surface may influence the electronic structures of the heterojunctions compared to the van der Waals heterostructures presented before. For that purpose, we consider the TiO₂ (101) bare and the TiO₂ (001) hydrated surfaces.

On the (101) surface, we optimized the interfacial system starting from a structure inspired by the one previously reported for Mo₆S_{12+x} clusters³¹⁻³². After optimization, the MoS₂ nanoribbon is tilted with an angle of ~40° between the Mo plane and the (101) surface. The interaction with the TiO₂ surface occurs through the so-called “Mo-edge” of MoS₂ whereas the opposite “S-edge” is free (Fig. 6 a). The stabilization at interface is ensured by 4 membered ring Mo-S-Ti-O. In the case of the hydrated (001) TiO₂ surface, we revisited the possible interactions of the two MoS₂ edges: the first one through the M-edge with an angle of ~58° (Fig. 6 b) and the second one through the S-edge with ~68° (Fig. 6 c). The interaction is ensured through Mo-O-Ti and Mo-S-Ti bridges in the first case and Mo-S-Ti-O rings in the second one. The adhesion energies calculated using the MoS₂ nanoribbon as a reference are - 0.24 eV / MoS₂ for the (101) surface, ~ 0 eV / MoS₂ for the (001) hydrated surface in interaction with the Mo-edge and -0.21 eV for the (001) hydrated surface interacting with the S-edge.

The DOS associated to the systems in chemical interaction (Fig. 6) illustrates the strong impact of the chemical interaction between the two semiconductors with large differences compared to the physical interaction. Although a bandgap is maintained, several localized and occupied states, localized on MoS₂, appears in the gap. If we compare the band positions before and after the junction (Fig. 6), the impact of the chemical bonds on the band structure is clearly visible with a large variation of the band positions. The effect on TiO₂ is visible only with the (101) surface with a small fall of the conduction band after interaction. On MoS₂, the impact is the same in all the cases, with a bandgap increased after the interaction and the apparition of these localized states. As illustrated by the spatial

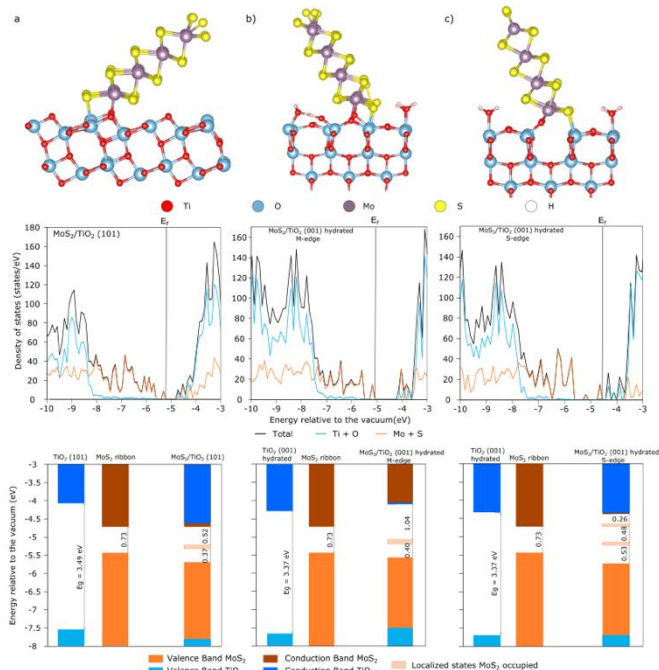


Fig. 6 Molecular structure of MoS₂ nanoribbon chemically adsorbed, DOS of the interfaces and evolution of the band position before and after junction for a) TiO₂ (101) b) TiO₂ (001) (interaction with M-edge) and c) TiO₂ (001) (interaction with S-edge)

charge analysis (**Supporting Information 6**), the occupied and unoccupied states (including localized states) close to the Fermi level are located either at the interface or at the free MoS₂ nanoribbon edge. In the case of the (101) surface (**Fig. S15**) and (001) surface (**Fig. S16**) in interaction with the S-edge, these localized states are at the interface whereas it is located at the free S-edge for the (001) surface in interaction with the M-edge (**Fig. S17**). Since the CB and VB of the materials are mainly localized at the interface (the only exception is with the (001) in interaction with the S-edge), the localized states at the interface could sadly become recombination centers.

The charge transfer mechanism involves a type I heterojunction with the valence band edge and conduction band edge that could be localized on MoS₂. Since the localized states could have unwished and complicated behaviors, including the accumulation of the holes and the diminution of the global bandgap, we explored if chemical modifications of the interface or size effect of the MoS₂ nanoribbon could change the type of heterojunction and avoid the apparition of such localized states in the bandgap.

b) Chemical modification of the 1D-interface

We have applied the same chemical modifications to the ribbon in chemical interaction with a TiO₂ surface as those applied on the nanoribbon alone (**Fig. 5**). Due to a significantly larger supercell of the (001) slab, these investigations have been undertaken on the (101) surface only.

The DOS associated to these structures clearly reveal the effect of these 3 chemical modifications on the electronic properties. The diminution of the number of Mo rows (**Fig. 7 a**) leads to a more complex electronic structure with a smaller bandgap and still localized states at the interface (**Fig. S18**) that could become

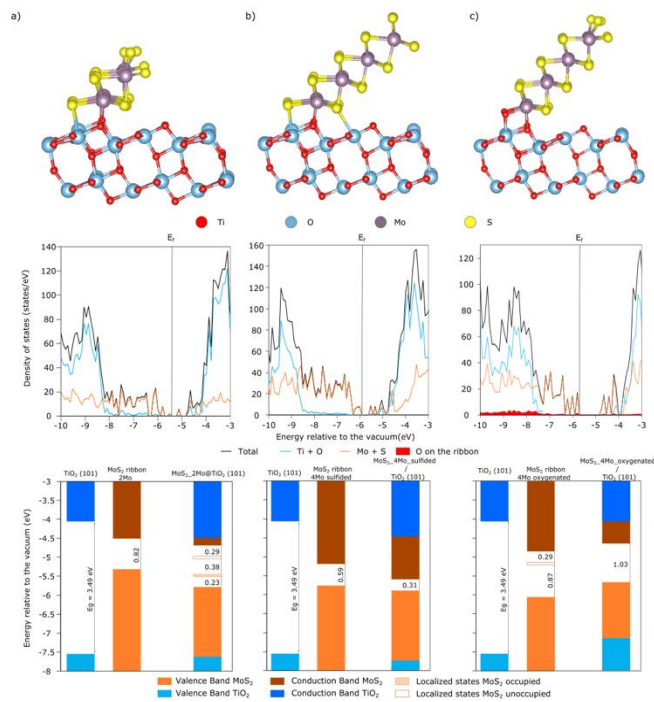


Fig. 7 Molecular structure of MoS₂ nanoribbon chemically adsorbed, DOS of the interfaces and evolution of the band position before and after junction for a) MoS₂ ribbon with 2 Mo rows b) MoS₂ ribbon with 4 Mo rows sulfided and c) MoS₂ ribbon with 4 Mo rows oxygenated.

recombination centers. In the cases of increased sulfidation at the free edge (**Fig. 7 b**) or oxygenation at the interface (**Fig. 7 c**), these localized states vanish. For the oxygenated interface, the bandgap is enlarged. In the sulfidation case (**Fig. S19**), the CB located at the free edge and the VB which contains contribution on both edges could lead to a spatial separation of the electrons and the holes generated. The same possibility occurs for oxygenated interface (**Fig. S20**), with a VB located at the interface and a CB with contribution on both edges. In the three cases, a type I heterojunction is found with the conduction band and the valence band both localized on MoS₂.

Discussion

The comparison of the band positions of all the physical interaction structures (**Fig. 8**) reveals that the strong modifications in the TiO₂ surface involves slight modifications in the band structures of MoS₂, because of the weak electronic interaction between the two materials. On the other hand, modifications in the band structure of TiO₂ could modify its electronic properties. On the (001) surface, while the hydration of the surface leads to an increase of TiO₂ bandgap in comparison with the bare surface (**Fig. S14 a**), the sulfidation of the surface involves a strong diminution of the band gap, with a significant upper shift of the valence band due to the 3p states of sulfur atoms at the top of the valence band. The same trend is observed with the sulfidation of the (101) surface. All cases correspond to a type II heterojunction, and two mechanisms ("classical" or "Z-scheme", **Fig. 1**) could be involved depending on the dynamics of charge carriers. On the one hand, the classical type II mechanism would imply the transfer of the holes in the VB of MoS₂, and the transfer of the electrons in the CB of

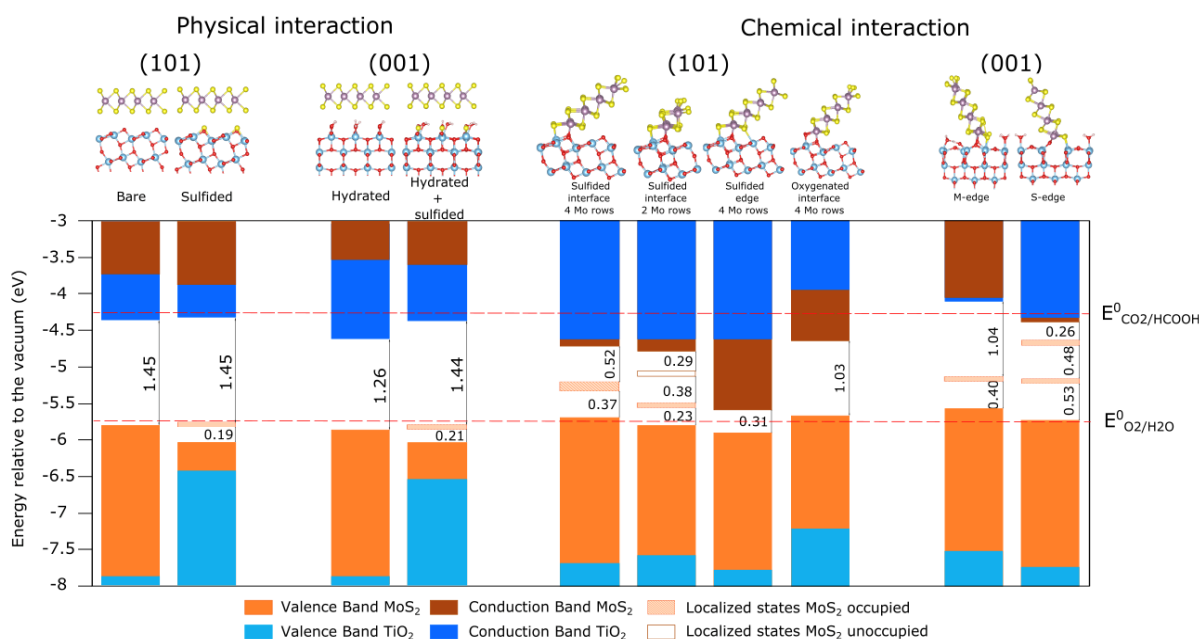


Fig. 8 Comparison of the band position of the two materials after junction for all the cases in physical interaction on the left and chemical interaction on the right

TiO₂. In that case, the reduction and oxidation potential are limited by the energy difference between the VB of MoS₂ and the CB of TiO₂. Alternatively, a Z-scheme mechanism would imply the recombination of the holes generated in MoS₂ with the electrons generated in TiO₂ at the interface (Fig. 9 a). This induces an accumulation of electrons in MoS₂ and holes in TiO₂. In these conditions, the system will exhibit appropriate reduction and oxidation potentials, that could allow to achieve the targeted photoreduction of CO₂ on MoS₂ and oxidation of H₂O on TiO₂.

The strong effect of the sulfidation on the electronic structure (diminution of TiO₂ bandgap and apparition of a localized state), could favor one of the two mechanisms as a function of the behavior of these localized states. Depending on the mechanism, MoS₂ will act as the reducer or as the oxidizer (TiO₂ will do the opposite reaction in both cases). This could be an argument in the choice of the mechanism. To do that, tuning by sulfidation the TiO₂ surface will be needed through the modification of the pressures of H₂S and H₂O during a pre-activation step of the material.

Although a clear conclusion about the mechanism that will take place in experiment ("classical" or "Z-scheme", Fig. 1) is impossible without the knowledge of dynamics of charge carriers, the distribution of charges at the interface and the resulting orientation of the internal electric field before irradiation might help to figure out if the junction will follow a classical or Z-scheme working principle Fig.9a¹⁴. Hence, the calculation of the Bader charge difference⁴⁸ between the sub-systems (MoS₂ nanosheet and TiO₂ surface) before and after junction has been performed (Table 1). In the case of physical interaction, a weak charge transfer occurs from one MoS₂ nanosheet to TiO₂, which is more significant with the (001) hydrated than with the (101) bare (+0.18 e⁻ vs +0.02 e⁻ per MoS₂ sheet). Obviously, the presence of H-bonding enhances the

transfer. Reversely, for both surfaces, the transfer is significantly attenuated by sulfidation of the (001) surface or even inverted for the (101) one (+0.07 e⁻ and -0.04 e⁻, respectively). As aforementioned, the presence of sulfur-atoms on TiO₂ surfaces induces an increase of the distance between the MoS₂ sheet and the surface. The fact that the junction involving the TiO₂ (001) hydrated surface induces such a negative charge on TiO₂ and a positive one on MoS₂ could generate the proper internal field with the expected band bending and facilitate a Z-scheme mechanism: the holes

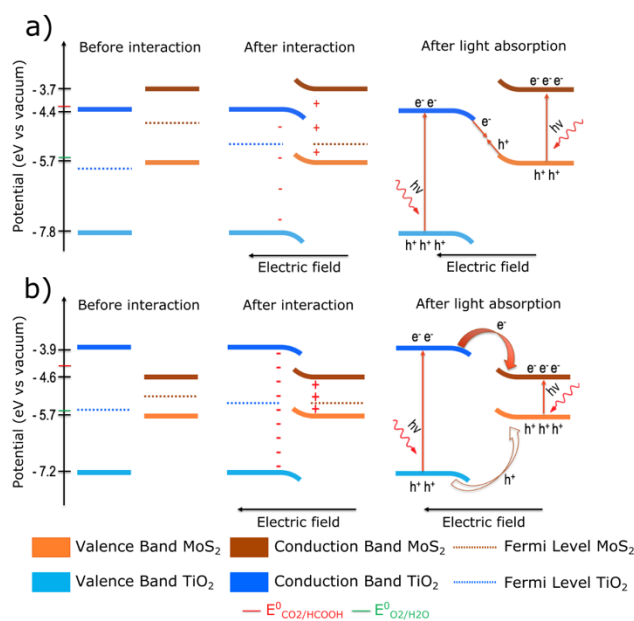


Fig. 9 a) Possible Z-scheme mechanism for the physical 2D-heterojunction between the MoS₂ sheet and the TiO₂ (101) surface, b) Type I heterojunction of the 1D chemical interface between MoS₂ nanoribbon (4 Mo rows oxygenated) and the TiO₂ (101) surface. Due to the intrinsic semiconductors involved, the Fermi levels are localized in the middle of the bandgap before interaction.

generated on MoS₂ are attracted by the negatively charged TiO₂ and the electrons generated on TiO₂ attracted by the positively charged MoS₂, leading to the targeted electron-hole recombination at the interface (**Fig.9 a**). Moreover, the band gap of the MoS₂/(001) TiO₂ hydrated heterojunction is 0.2 eV smaller than the one of MoS₂/(101) TiO₂ which is also a parameter in favor of a Z-scheme mechanism. Hence, the stabilization of a heterojunction involving the hydrated (001)

Interaction type	Structure	Δe^- MoS ₂ (per nanosheet)	Δe^- TiO ₂
2D-Physical	(101) bare	- 0.02	+ 0.04
	(101) sulfided	+ 0.04	- 0.09
	(001) hydrated	- 0.18	+ 0.36
	(001) hydrated-sulfided	- 0.07	+ 0.15
1D-Chemical	(101) 4 Mo rows	- 0.52	+1.04
	(101) 2 Mo rows	- 0.62	+ 1.25
	(101) sulfided edge	- 0.51	+ 1.02
	(001) oxygenated interface	- 0.19	+ 0.39
	(001) Mo-edge	- 0.22	+ 0.44
	(001) S-edge	+ 0.14	- 0.28

Table 1 Fraction of electron transferred from MoS₂ (i.e. a negative value indicates a loss of electron)⁴⁸

surface without sulfidation should be sought at the synthesis step. This result might explain in part the recent experimental studies on 2D-2D MoS₂/(001) TiO₂ nanojunctions³⁰ revealing a H₂ evolution rate 36.4 times higher than that of pure TiO₂. Our calculations show that the charge transfer thanks to a surface contact increases which could be explained by a Z-scheme mechanism enhancing a spatial separation of the charge carriers while maintaining a good reduction and oxidation power.

If we now summarize the band positions of all systems in chemical interaction (**Fig. 8**), the various MoS₂ nanoribbons lead to modifications on the electronic structure of both materials. In fact, while the modification of the number of rows and the modification of the edge leads logically to slight modifications in the band positions, the sulfur/oxygen exchange at the interface implies the modification of the interaction with the TiO₂ surface and an increase of its conduction band and valence band. Concerning MoS₂, the modification of the number of rows and the sulfidation at the edge narrow the bandgap and eliminate the localized state in the gap. It is accompanied by a shift to the lowest energy in the second case.

In the case of the oxygenated interface, the substitution of the sulfur at the interface has a low impact on MoS₂ electronic structure apart the vanishing of the localized states. Concerning the charge transfer analysis (**Table 1**), we observe once again an electron transfer from MoS₂ to TiO₂, except in the case with the ribbon in interaction with its S-edge. As expected, the charge transfer is stronger than with the physical interaction (higher than 0.5 electron by nanosheet in 3 cases). The strongest charge transfer occurs for the MoS₂ nanoribbon of smaller size (2 Mo rows) which may be explained by the strong delocalization of charge within the nanoribbon (**Fig. S18**). Reversely, the charge transfer is limited by the presence of oxygen near the surface (+0.20 for the (101) with oxygenated interface and + 0.22 for the ribbon on the (001) hydrated) which is consistent with the

large band gap observed for this system. The impact of the electric field induced by this charge transfer on type I heterojunction can be discussed from **Fig.9 b**. Due to their respective band positions, these systems could lead to the accumulation of both electrons and holes in the conduction band and valence band of MoS₂. In this case, the material should have limited applications as heterojunctions for photocatalysis, particularly in the case of the CO₂ photoreduction. In these systems, MoS₂ should be considered mainly as a co-catalyst. Nevertheless, due to the induced electric field, the hole transfer facing a barrier could be limited. We cannot rule out the possibility that, due to this barrier, the holes remain on TiO₂ which would imply certain potential interest for photocatalytic applications due to good charge separation between TiO₂ and MoS₂: H₂O being oxidized on TiO₂ and CO₂ being reduced on MoS₂ (although the CB level might be slightly insufficient).

Conclusions

Thanks to state of the art DFT calculations including HSE06 functional, we showed how the various possible structural modifications of the MoS₂/TiO₂ heterojunction impact the resulting electronic properties: band gaps and CB/VB band positions. In particular, we distinguished the effects of a physical interaction and a chemical one between the MoS₂ and TiO₂ materials on the nature of the MoS₂/TiO₂ heterojunctions. A physical 2D-interface may lead to a type II or Z-scheme formalism. The analysis of the CBE/VBE band positions revealed that the physical interaction is compatible with a photocatalytic reduction process of CO₂. Moreover, a weak but non-negligible charge transfer occurs from the MoS₂ nanosheet to the hydroxylated (001) surface of TiO₂ which may induce of a Z-scheme mechanism more efficient for photon absorption processes in photocatalysis applications with reduction of CO₂ on MoS₂ and oxidation of H₂O on TiO₂. The sulfidation of the TiO₂ surface does not improve the resulting electronic properties. By contrast, all chemical 1D-interfacial systems between MoS₂ nanoribbons and TiO₂ surfaces imply the formation of a type I heterojunction. The chemical interaction induces a stronger charge transfer at the interface than for the physical interaction but the type I mode will not obligatory enhance the photon absorption efficiency during photocatalysis, except if the barrier for the hole transfer is too high and constrains the hole on TiO₂ while electrons are transferred to MoS₂.

We hope that our theoretical work quantifying the sensitivity of the electronic properties with respect to atomic scale modifications of the MoS₂/TiO₂ heterostructure will help to provide more rational guides to tune such heterojunction. A perspective of this work would be to evaluate the efficiency of these interfaces to perform the photocatalytic CO₂ reduction either by using the Computational Hydrogen Electrode⁴⁹⁻⁵⁰ or even using the Grand Canonical DFT⁵¹.

Author Contributions

P. R. and T. L. B. designed the research plan. R. F. conducted the DFT calculations and drafted the manuscript. P. R. and T. L. B. supervised the thesis research. All authors participated data analysis and manuscript writing.

Conflicts of interest

There are no conflicts to declare.

Acknowledgements

This work is part of the “RatiOnAl Design for CATalysis” (ROAD4CAT) industrial chair, project IDEXLYON funded by the French National Research Agency (ANR-16-IDEX-0005) and the Commissariat-General for Investment (CGI) within the framework of Investissements d’Avenir program (“Investment for the future”). The authors thank the SYSPROD project and AXELERA Pôle de Compétitivité for financial support (PSMN Data Center). This work was granted access to the HPC resources of CINES, IDRIS and TGCC under the allocation 2018-080609 made by GENCI.

References

- 1 A. Kudo and Y. Miseki, *Chem. Soc. Rev.*, 2009, **38**, 253-278.
- 2 M. G. Walter, E. L. Warren, J.R. McKone, S. W. Boettcher, Q. Mi, E. A. Santori and N. S. Lewis, *Chem. Rev.*, 2010, **110**, 6446-6473.
- 3 X. C. Chen, S. Shen, L. Guo and S. S. Mao, *Chem. Rev.*, 2010, **110**, 6503-6570.
- 4 W. Tu, Y. Zhou and Z. Zou, *Adv. Mater.*, 2014, **26**, 4607-4626.
- 5 X. Chang, T. Wang and J. Gong, *Energy Environ. Sci.*, 2016, **9**, 2177.
- 6 U. Kang, D. S. Han, S. K. Choi, D. J. Ham, S. M. Ji, W. Choi, D. S. Han, A. Abdel-Wahab and H. Park, *Energy Environ. Sci.*, 2015, **8**, 2638.
- 7 U. Ulmer, T. Dingle, P. N. Duchesne, R. H. Morris, A. Tavasoli, T. Wood and G. A. Ozin, *Nature Commun.*, 2019, 1-12.
- 8 A. B. Laursen, S. Kegnaes, S. D. Dahl and I. Chorkendorff, *Energy Environ. Sci.*, 2012, **5**, 5577.
- 9 L. Qian, Z. Ning, Y. Yong, W. Guozhong and H. L. N. Dickon, *Langmuir*, 2014, **30**, 8965-8972.
- 10 M. Shahrokhi, P. Raybaud and T. Le Bahers, *J. Mater. Chem. C*, 2020, **8**, 4920-4935.
- 11 A. R. Beal and H. P. Hughes, *J. Phys. C: Solid State Phys.*, 1979, **12**, 881-890.
- 12 K. F. Mak, C. Lee, J. Hone, J. Shan and T. F. Heinz, *Phys. Rev. Lett.*, 2010, **105**, 136805.
- 13 P. Zhou, J. Yu and M. Jaroniec, *Adv. Mater.*, 2014, **26**, 4920-4935.
- 14 X. Li, C. Garlisi, Q. Guan, S. Anwer, K. Al-Ali, G. Palmisano and L. Zheng, *Materials Today*, 2021, **47**, 75-107.
- 15 B. Chen, Y. Meng, J. Sha, C. Zhong, W. Hu and N. Zhao, *Nanoscale*, 2018, **10**, 34-68.
- 16 C. Maheu, E. Puzenat, C. Geantet, L. Cardenas and P. Afanasiev, *Inter. Journ. Hydr. Energy*, 2019, **44**, 18038-18049.
- 17 A. Fujishima, X. Zhanj and D. A. Tryk, *Surf. Sci. Rep.*, 2008, **63**, 515-582.
- 18 A. L. Linsebigler, G. Lu and J. T. Yates Jr, *Chem. Rev.*, 1995, **95**, 735-758.
- 19 C. G. Morales-Guio, L-A. Stern and X. Hu, *Chem. Soc. Rev.*, 2014, **43**, 6555-6569.
- 20 B. Baubet, M. Girleanu, A-S. Gay, A-L. Taleb, M. Moreaud, F. Wahl, V. Delattre, E. Devers, A. Hugon, O. Ersen, P. Afanasiev and P. Raybaud, *ACS Catal.*, 2016, **6**, 1081-1092.
- 21 W. Zhang, X. Xiao, Y. Li, X. Zheng, L. Zheng and C. Whan, *RSC Adv.*, 2016, **6**, 33705-33712.
- 22 X. Liu, Z. Xing, H. Zhang, W. Wang, Y. Zhang, Z. Li, X. Wu, X. Yu and W. Zhou, *Chem. Sus. Chem.*, 2016, **9**, 1118-1124.
- 23 W. Tu, Y. Li, L. Kuai, Y. Zhou, Q. Xu, H. Li, X. Wang, M. Xiao and Z. Zou, *Nanoscale*, 2017, **9**, 9065-9070.
- 24 S. Kanda, T. Akita, M. Fujishima and H. Tada, *J. Colloid Interf. Sci.*, 2011, **354**, 607-610.
- 25 M. Shen, Z. Yan, L. Yang, P. Du, J. Zhang and B. Xiang, *Chem. Commun.*, 2014, **50**, 15447-15449.
- 26 W. Zhou, Z. Yin, Y. Du, X. Huang, Z. Zeng, Z. Fan, H. Liu, J. Wang and H. Zhang, *Small*, 2013, **9**, 140-147.
- 27 X. Zhou, M. Lickleder and P. Schmuki, *Electrochem. Commun.*, 2016, **73**, 33-37.
- 28 M. Lazzeri, A. Vittadini and A. Selloni, *Phys. Rev. B*, 2001, **63**, 155409.
- 29 C. Arrouvel, M. Digne, M. Breyse, H. Toulhoat and P. Raybaud, *J. Catal.*, 2004, **222**, 152-166.
- 30 Y-J. Yuan, Z-J. Ye, H. Lu, B. Hu, Y-H. Li, D. Chen, J-S. Zhong, Z-T. Yu and Z. Zou, *ACS Catal.*, 2015.
- 31 C. Arrouvel, M. Breyse, H. Toulhoat and P. Raybaud, *J. Catal.*, 2005, **232**, 161-178.
- 32 D. Costa, C. Arrouvel, M. Breyse, H. Toulhoat and P. Raybaud, *J. Catal.*, 2007, **246**, 325-343.
- 33 Y. Sakashita, Y. Araki, K. Honna and H. Shimada, *Appl. Catal. A.*, 2000, **197**, 247-253.
- 34 G. Kresse and J. Furthmüller, *Comput. Mater. Sci.*, 1996, **6**, 15-50.
- 35 G. Kresse and J. Furthmüller, *Phys. Rev. B*, 1996, **54**, 11169-11186.
- 36 J. P. Perdrew, K. Burke and M. Ernzerhof, *Phys. Rev. Lett.*, 1996, **77**, 3865-3868.
- 37 J. Heyd and G. E. Scuseria, *J. Chem. Phys.*, 2004, **121**, 1187-1192.
- 38 S. Grimme, S. Ehrlich and L. Goerigk, *J. Comp. Chem.*, 2011, **32**, 1456-1465.
- 39 K. Matthew, R. Sundararaman, K. Letchworth-Weaver, T. A. Arias and R. G. Hennig, *J. Chem. Phys.*, 2014, **140**, 084106.
- 40 J. Kullgren, B. Aradi, T. Frauenheim, L. Kavan and P. Deak, *J. Phys. Chem. C*, 2015, **119**, 21952-21958.
- 41 H. Han, K. M. Kim, C-W. Lee, C. S. Lee, R. C. Pawar, J. L. Jones, Y-R. Hong, J. H. Ryu, T. Song, S. H. Kang, H. Choi and S. Mhin, *Phys. Chem. Chem. Phys.*, 2017, **19**, 28207-28215.
- 42 C. Arrouvel, H. Toulhoat, M. Breyse and P. Raybaud, *J. Catal.*, 2004, **226**, 260-272.
- 43 L. Coulier, J. van Veen and J. Niemantsverdriet, *Catal. Lett.*, 2002, **79**, 149-155.
- 44 H. Schweiger, P. Raybaud, G. Kresse and H. Toulhoat, *J. Catal.*, 2002, **207**, 76-87.
- 45 P. Raybaud, J. Hafner, G. Kresse, S. Kasztelan and H. Toulhoat, *J. Catal.*, 2000, **189**, 129-146.
- 46 R. G. Leliveld, A. J. van Dillen, J. W. Geus and D. C. Koningsberger, *J. Catal.*, 1997, **165**, 184-196.
- 47 B. Baubet, A-S. Gay, A-L. Taleb, M. Moreaud, F. Wahl, V. Delattre, E. Devers, A. Hugon, O. Ersen, P. Afanasiev and P. Raybaud, *ACS Catal.*, 2016, **6**, 1081-1092.
- 48 R.F.W. Bader, *New York: Oxford university press*, 1990.
- 49 M. Bajdich, M. Garcia-Mota, A. Vojvodic, J. K. Nørskov and A. T. Bell, *J. Am. Chem. Soc.*, 2013, **135**, 13521-13530.
- 50 L. Lv, Y. Shen, X. Gao, J. Liu, S. Wu, Y. Ma, X. Wang, D. Gong, Z. Zhou, *Appl. Surf. Sci.*, 2021, **546**, 149066.
- 51 A. Curutchet, P. Colinet, C. Michal, S. N. Steinmann and T. Le Bahers, *Phys. Chem. Chem. Phys.*, 2020, **22**, 7031-7038.